Journal of Rock Mechanics and Geotechnical Engineering 15 (2023) 1391–1405

Contents lists available at ScienceDirect

Journal of Rock Mechanics and Geotechnical Engineering

journal homepage: www.jrmge.cn

Full Length Article

Estimation of fracture size and azimuth in the universal elliptical disc model based on trace information

Jichao Guo [a], Jun Zheng [a,*], Qing Lü [a], Jianhui Deng [b]

[a] Department of Civil Engineering, Zhejiang University, Hangzhou, 310058, China
[b] State Key Laboratory of Hydraulics and Mountain River Engineering, College of Water Resource and Hydropower, Sichuan University, Chengdu, 610065, China

ARTICLE INFO

Article history:
Received 6 May 2022
Received in revised form
19 June 2022
Accepted 17 July 2022
Available online 13 September 2022

Keywords:
Universal elliptical disc (UED) model
Rock mass
Discrete fracture network (DFN)
Optimization algorithm
Inverse problem

ABSTRACT

The geometric characteristics of fractures within a rock mass can be inferred by the data sampling from boreholes or exposed surfaces. Recently, the universal elliptical disc (UED) model was developed to represent natural fractures, where the fracture is assumed to be an elliptical disc and the fracture orientation, rotation angle, length of the long axis and ratio of short-long axis lengths are considered as variables. This paper aims to estimate the fracture size- and azimuth-related parameters in the UED model based on the trace information from sampling windows. The stereological relationship between the trace length, size- and azimuth-related parameters of the UED model was established, and the formulae of the mean value and standard deviation of trace length were proposed. The proposed formulae were validated via the Monte Carlo simulations with less than 5% of error rate between the calculated and true values. With respect to the estimation of the size- and azimuth-related parameters using the trace length, an optimization method was developed based on the pre-assumed size and azimuth distribution forms. A hypothetical case study was designed to illustrate and verify the parameter estimation method, where three combinations of the sampling windows were used to estimate the parameters, and the results showed that the estimated values could agree well with the true values. Furthermore, a hypothetical three-dimensional (3D) elliptical fracture network was constructed, and the circular disc, non-UED and UED models were used to represent it. The simulated trace information from different models was compared, and the results clearly illustrated the superiority of the proposed UED model over the existing circular disc and non-UED models.

1. Introduction

Rock engineering is closely related to geological disaster prevention (Dershowitz and Einstein, 1988; Zheng et al., 2014a; Ma and Liu, 2022), civil and hydraulic engineering construction (Cacas et al., 1990; Kulatilake et al., 1997; Baghbanan and Jing, 2007; Pan et al., 2016; Zhang et al., 2021), mineral development (Ajayi and Schatzel, 2020; Chen et al., 2021), and underground oil storage construction (Li et al., 2016; Shaunik and Singh, 2020; Fan et al., 2021). The main reason for the complex rock mass properties, i.e. discontinuity, heterogeneity and anisotropy, is the existence of numerous fractures in a rock mass (ISRM, 1978; Priest, 1993). How to describe the geometric characteristics of fractures accurately by rock mass structure models is critical for the quantitative analysis on rock mass behaviors. At present, it is recognized that the most effective way to quantitatively characterize the geometries of discontinuities is to construct a three-dimensional (3D) discrete fracture network (DFN) (Chilès, 1988; Dershowitz and Einstein, 1988; Kulatilake et al., 1993; Zhang et al., 2020; Zheng et al., 2020; Guo et al., 2021). Since most fractures are within the rock mass, it is widely accepted to infer the 3D geometric characteristics of fractures from one-dimensional (1D) measurements sampled along scanlines or in boreholes and/or two-dimensional (2D) measurements sampled on tunnel walls or natural outcrops. Based on the measurements, the 3D DFN models can be developed (Warburton, 1980a, b; Kulatilake et al., 1990; Villaescusa and Brown, 1992; Kulatilake et al., 1993; Kemeny and Post, 2003; Priest, 2004; Song, 2006; Wu et al., 2011; Zheng et al., 2017).

The primary step of constructing DFNs is to describe the fracture with a defined shape, i.e. circle, ellipse (Baecher et al., 1977; Barton,

* Corresponding author.
E-mail address: zhengjun12@zju.edu.cn (J. Zheng).
Peer review under responsibility of Institute of Rock and Soil Mechanics, Chinese Academy of Sciences.

https://doi.org/10.1016/j.jrmge.2022.07.018

Table 1
Existing research on different fracture models.

Model	Basic assumption	Size characteristic parameter	Reference
Circular disc	Fractures are planar	Diameter	Warburton (1980a); Villaescusa and Brown (1992); Zhang and Einstein (2000); Song (2006)
Similar parallelogram	Fractures are planar and parallel; a constant ratio of long to short sides	Length of the sides	Warburton (1980b)
Non-UED	Fractures are planar and parallel; a constant ratio of long-short axis lengths; Constant direction of the long axis	Length of the long axis	Zhang et al. (2002)
	Fractures are planar; a constant ratio of long-short axis lengths; Constant direction of the long axis		Jin et al. (2014); Gao et al. (2016)
UED	Fractures are planar	Length of the long axis, ratio of short-long axis lengths, direction of the long axis	This study

1978), parallelogram (Warburton, 1980b) and polygon (Ivanova, 1998). Owing to its mathematical simplicity, the circular disc model has become the most widely used one (Warburton, 1980a; Priest, 2004). With respect to the real shape of fracture, Petit et al. (1994) studied the fully exposed fracture plane and found that its shape is more likely to be an ellipse than a circle. Zhang and Einstein (2010) concluded that fractures usually tend to be rectangular under the circumstances of intersecting geological structures and elliptical with no affecting factor. Hence, the applicability of the circular disk model is limited. Recently, the elliptical fracture model has been modified to approximately represent circles or polygons (Zhang et al., 2002; Jin et al., 2014). Since the elliptical disc model has more than one size- or azimuth-related parameters, for simplicity, the ratio of short-long axis length (defined as the ratio of short to long axis length of the ellipse) and the direction of the long axis are set to be constant. This type of elliptical disc model can only be applied to rock masses, and hence it is called the non-universal elliptical disc (non-UED) model. For this, Zheng et al. (2022) have developed a UED model, considering the variances of the direction of the long axis and ratio of short-long axis lengths. In addition, Zheng et al. (2022) concluded that the accuracy representation index (*ARI*) of the UED model was approximately 20% higher than that of the non-UED model (Guo et al., 2020). Therefore, the UED model is worth being considered and applied to engineering.

To construct DFN using UED model, it is essential to infer the characteristic geometric parameters of the UED model based on 1D or 2D measurements. With respect to the trace exposure, the relevant studies on estimating the size- or azimuth-related parameters based on the trace information are summarized in Table 1. In this study, the elliptical fracture size- and azimuth-related parameters are inferred from the trace length on different sampling windows, while the UED model is used to describe the fractures.

2. A brief introduction of the UED model

The UED model has been developed by Zheng et al. (2022), and the following geometric characteristics are regarded as variables in this model: (1) the central point; (2) the azimuth including the dip direction, dip angle, and direction of the long axis; and (3) the size-related parameters including the length of the long axis and the ratio of short-long axis lengths. The fundamental assumptions are: (1) all fractures are planar, (2) the central point of the fractures has a Poisson distribution with the 3D density of P_{30}, and (3) the parameters related to the center, azimuth and size are independent.

As shown in Fig. 1, an elliptical fracture can be described by the following geometric parameters (Zheng et al., 2022): (1) location of its center, O; (2) length of the long axis, a; (3) ratio of short-long axis lengths, k; (4) dip angle, δ; (5) dip direction, θ; and (6) rotation angle, γ. It should be noted that γ is the angle between the direction of the downward long axis ($\boldsymbol{l}_e$) and that of the downward maximum slope line ($\boldsymbol{m}_{sle}$) on the fracture plane, which is used to describe the direction of the long axis (Zheng et al., 2022). The range of γ is from $-\pi/2$ to $\pi/2$. When $\boldsymbol{m}_{sle}$ rotates counterclockwise to $\boldsymbol{l}_e$, γ is positive and negative otherwise.

3. Derivation and validation of trace length of UED model

Based on the aforementioned descriptions and assumptions of the UED model, the forward derivation and inverse estimation of the analysis is shown in Fig. 2. To solve the inverse problem, we need to make a forward derivation first, i.e. we estimate the relationship between the trace length and the geometric parameters of a 3D discrete universal elliptical fracture network. The following forward derivation is made based on stereology.

3.1. Derivation

As shown in Fig. 3a, considering a unit area of the sampling window plane with a dip direction of θ_s and a dip angle of δ_s, an elliptical facture labeled as E with a dip direction of θ and a dip angle of δ is intersected by the sampling window plane, and the dihedral angle between the sampling window and the elliptical fracture plane is denoted as ε. It should be noted that ε is an acute dihedral angle and ranges from 0 to $\pi/2$. Since θ, δ, θ_s and δ_s are in the geological coordinate system, they are converted into the polar coordinate system labeled as α, β, αs and βs, respectively by the following equations (Zheng et al., 2014b):

$$\beta = \delta \tag{1a}$$

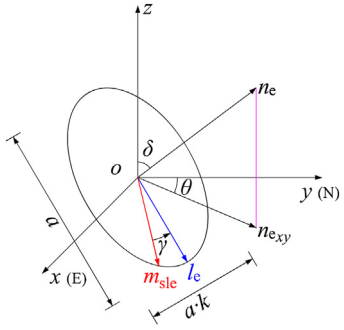

Fig. 1. Parameters of the UED model (after Zheng et al., 2022).

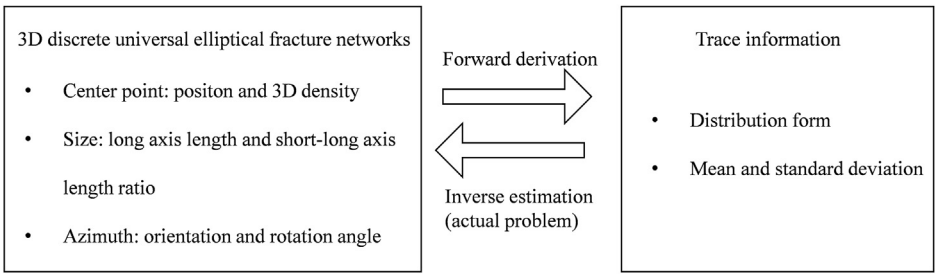

Fig. 2. Forward derivation and inverse estimation of the UED model.

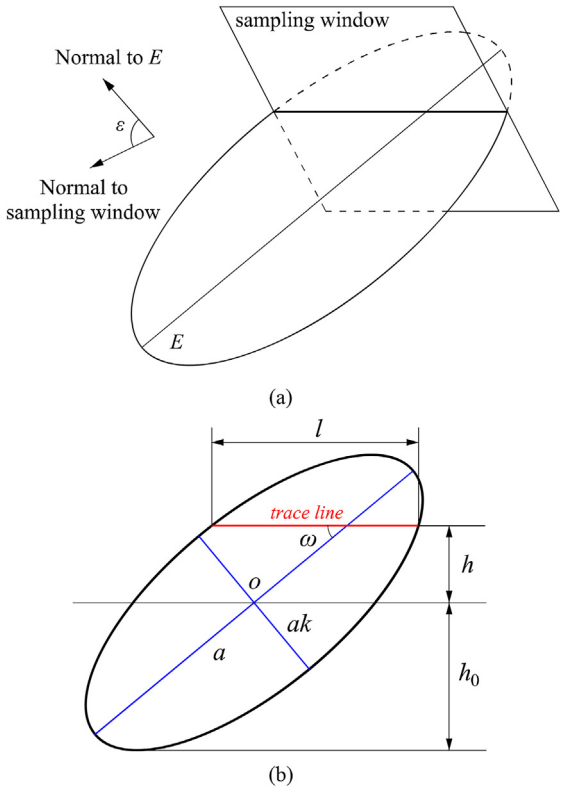

Fig. 3. Parameters of the elliptical fracture plane that is intersected by the sampling window: (a) Dihedral angle ε between the elliptical fracture plane and the sampling window, and (b) Parameters of the trace line and the elliptical fracture.

$$\alpha = \begin{cases} \frac{\pi}{2} - \theta & \left(\theta \le \frac{\pi}{2}\right) \\ \frac{5\pi}{2} - \theta & \left(\theta > \frac{\pi}{2}\right) \end{cases} \tag{1b}$$

The normal vectors of E and sampling window plane labeled as $\boldsymbol{n}_e$ and $\boldsymbol{n}_s$ can be calculated as

$$\boldsymbol{n}_e = [\sin\beta\cos\alpha \;\; \sin\beta\sin\alpha \;\; \cos\beta] \tag{2}$$

$$\boldsymbol{n}_s = [\sin\beta_s\cos\alpha_s \;\; \sin\beta_s\sin\alpha_s \;\; \cos\beta_s] \tag{3}$$

and then ε can be obtained by the dot product of $\boldsymbol{n}_e$ and $\boldsymbol{n}_s$ as

$$\varepsilon = \arccos(|\sin\beta\cos\alpha\sin\beta_s\cos\alpha_s + \sin\beta\sin\alpha\sin\beta_s\sin\alpha_s + \cos\beta\cos\beta_s|) \tag{4}$$

As shown in Fig. 3b, a trace line of length l exists at the intersection between fracture E and the sampling window. l is related to the length of the long axis a, the ratio of short-long axis lengths k, the distance h between the fracture center to the trace line, and the angle ω between the trace line and the long axis. Due to symmetry, ω ranges from 0 to π. The calculation of l can be expressed as (modified after Zhang et al., 2002):

$$l = \frac{2k\sqrt{\tan^2\omega + 1}\sqrt{(a/2)^2\left(\tan^2\omega + k^2\right) - h^2\left(\tan^2\omega + 1\right)}}{\tan^2\omega + k^2} \tag{5}$$

It is worth noting that the definition of k is different from that given by Zhang et al. (2002). When the trace line is tangent to the edge of the ellipse, i.e. $l = 0$, h reaches the maximum value of h_0 as

$$h_0 = \frac{a\sqrt{\tan^2\omega + k^2}}{2\sqrt{\tan^2\omega + 1}} \tag{6}$$

As shown in Fig. 4, a parallelepiped was constructed using the unit sampling window and fracture E. The front and back surfaces of the parallelepiped need to bound the fracture E, with the distance defined as $2h_0\cos\psi$, where ψ is the angle between the elliptical fracture plane and the plane perpendicular to the sampling window, which is equal to $\pi/2-\varepsilon$. The significance of constructing the parallelepiped is that a trace line with a midpoint in the unit sampling window can be produced only when the centers of fractures with the same size and azimuth characteristics are located in the parallelepiped. Hence, the number of the midpoints within the unit sampling window (N_t) equals the total number of the fracture centers in the parallelepiped, as

$$N_t = P_{30}\frac{\sqrt{\tan^2\omega + k^2}}{\sqrt{\tan^2\omega + 1}}a\cos\psi \tag{7}$$

A fraction $g(a)\mathrm{d}a g(k)\mathrm{d}k g(\omega)\mathrm{d}\omega f(\alpha,\beta)\mathrm{d}\alpha\mathrm{d}\beta$ of fractures with a, k, ω, α, β in the ranges of a–a+da, k–k+dk, ω–ω+dω, α–α+dα, β–β+dβ is considered to be typical elliptical fractures, where $g(a)$ is the probability density function (PDF) of a, $g(k)$ is the PDF of k, $g(\omega)$ is the PDF of ω, and $f(\alpha,\beta)$ is the 2D PDF of α and β. The average number N_a of trace midpoints per unit area equals the average number of such elliptical fractures with the centers located in the parallelepipeds, as

$$N_a = P_{30}\frac{\sqrt{\tan^2\omega + k^2}}{\sqrt{\tan^2\omega + 1}}a\cos\psi g(a)\mathrm{d}a g(k)\mathrm{d}k g(\omega)\mathrm{d}\omega f(\alpha,\beta)\mathrm{d}\alpha\mathrm{d}\beta \tag{8}$$

Integrating Eq. (8) over the ranges of all possible a, k, ω, α and β, the average total number of trace midpoints per unit area labeled as P_{20} is given by

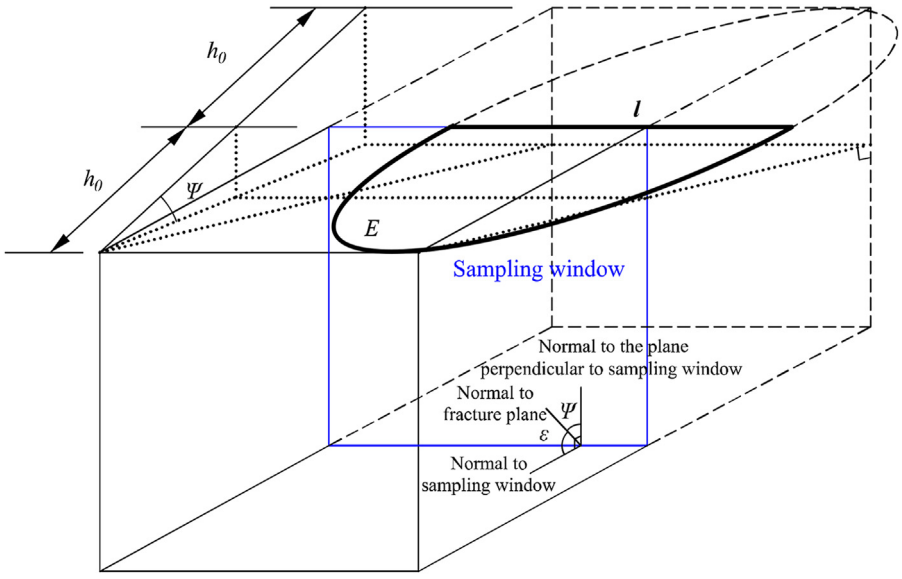

Fig. 4. Schematic diagram of the relationship between the elliptical fracture plane and the sampling window plane (revised after Zhang et al., 2002).

$$P_{20} = \int_0^{+\infty}\int_0^{1}\int_0^{\pi}\int_0^{2\pi}\int_0^{\pi} P_{30}\frac{\sqrt{\tan^2\omega + k^2}}{\sqrt{\tan^2\omega + 1}} a\cos\psi g(a)\mathrm{d}a g(k)\cdot \mathrm{d}k g(\omega)\mathrm{d}\omega f(\alpha,\beta)\mathrm{d}\alpha\mathrm{d}\beta \tag{9}$$

For simplicity, λ, τ and μ_a are defined as

$$\lambda = \int_0^{2\pi}\int_0^{\pi} \cos\psi f(\alpha,\beta)\mathrm{d}\alpha\mathrm{d}\beta \tag{10}$$

$$\tau = \int_0^{\pi}\int_0^{1} \frac{\sqrt{\tan^2\omega + k^2}}{\sqrt{\tan^2\omega + 1}} g(k)\mathrm{d}k g(\omega)\mathrm{d}\omega \tag{11}$$

$$\mu_a = \int_0^{+\infty} a g(a)\mathrm{d}a \tag{12}$$

where λ and τ are the codes with no practical significance; and μ_a represents the mean value of the length of the long axis. Hence, Eq. (9) can be rewritten as

$$P_{20} = P_{30}\lambda\tau\mu_a \tag{13}$$

Dividing Eq. (8) by Eq. (13), the fraction of traces produced by elliptical fractures labeled as P_t is obtained as

$$P_t = \frac{\sqrt{\tan^2\omega + k^2}}{\lambda\tau\mu_a\sqrt{\tan^2\omega + 1}} a g(a)\mathrm{d}a g(k)\mathrm{d}k g(\omega)\mathrm{d}\omega\cos\psi f(\alpha,\beta)\mathrm{d}\alpha\mathrm{d}\beta \tag{14}$$

As shown in Fig. 3b, the trace line is located at a distance of h from the fracture center. Since the fracture centers are randomly and uniformly distributed in the volume, the distance h is uniformly distributed in the range of 0–h_0. The elliptical fractures with the ranges of a–a+da, k–k + dk, ω–ω+dω, α–α+dα, β–β+dβ intersected by the sampling plane have a constant density as ρ, expressed as

$$\rho = \frac{1}{h_0} = \frac{2\sqrt{\tan^2\omega + 1}}{a\sqrt{\tan^2\omega + k^2}} \tag{15}$$

The fraction of fracture centers located at a distance of h–h+dh from their intersections with the sampling plane, which is labeled as P_h, is given by

$$P_h = \frac{2\sqrt{\tan^2\omega + 1}}{a\sqrt{\tan^2\omega + k^2}}\mathrm{d}h \tag{16}$$

Combining Eqs. (14) and (16), the fraction of traces produced by fractures in the ranges of a–a+da, k–k+dk, ω–ω+dω, α–α+dα, β–β+dβ, as well as central locations in the range of h–h+dh, which is labeled as P_{th}, is as follows:

$$P_{th} = \frac{2g(a)\mathrm{d}a g(k)\mathrm{d}k g(\omega)\mathrm{d}\omega\cos\psi f(\alpha,\beta)\mathrm{d}\alpha\mathrm{d}\beta\mathrm{d}h}{\tau\lambda\mu_a} \tag{17}$$

According to the relationship between l and h in Eq. (5), it can be transformed into a new equation with l as the variable. The derivative of h over l can be expressed as follows:

$$\mathrm{d}h = \frac{-\left(\tan^2\omega + k^2\right)l\mathrm{d}l}{2k(\tan^2\omega + 1)\sqrt{\frac{k^2(\tan^2\omega+1)}{\tan^2\omega+k^2}a^2 - l^2}} \tag{18}$$

where the minus sign in the numerator means that h decreases with the increase of l and the minus sign can be omitted.

Combining Eqs. (17) and (18), the fraction of total traces that have lengths between l and l+dl produced by elliptical fractures in the ranges from a–a+da, k–k+dk, ω–ω+dω, α–α+dα, β–β+dβ, which is labeled as P_l, can be obtained by

$$P_l = \frac{\left(\tan^2\omega + k^2\right) l \mathrm{d}l g(a)\mathrm{d}a g(k)\mathrm{d}k g(\omega)\mathrm{d}\omega \cos\psi f(\alpha,\beta)\mathrm{d}\alpha\mathrm{d}\beta}{\lambda\tau\mu_a k(\tan^2\omega+1)\sqrt{\frac{k^2(\tan^2\omega+1)}{\tan^2\omega+k^2}a^2 - l^2}} \tag{19}$$

In Eq. (5), when $h = 0$, l reaches its maximum value by

$$l_{\max} = \sqrt{\frac{k^2(\tan^2\omega+1)}{\tan^2\omega+k^2}}a \tag{20}$$

It can be seen that only when the length of the long axis a is larger than $l/[k^2(\tan^2\omega+1)/(\tan^2\omega+k^2)]^{1/2}$, the elliptical fractures will produce traces of length between l and $l + \mathrm{d}l$. The total number of traces (N_l) that have lengths between l and $l + \mathrm{d}l$ can be obtained by integrating Eq. (19) with a, k, ω, α, β in the ranges of $[l/[k^2(\tan^2\omega+1)/(\tan^2\omega+k^2)]^{1/2}, +\infty)$, [0, 1], [0, π], [0, 2π], [0, π], respectively, as

$$N_l = \frac{l\mathrm{d}l}{\lambda\tau\mu_a}\int_0^1 g(k)\mathrm{d}k\int_0^\pi g(\omega)\mathrm{d}\omega \int_{l\Big/\sqrt{\frac{k^2(\tan^2\omega+1)}{\tan^2\omega+k^2}}}^{+\infty} \frac{\left(\tan^2\omega+k^2\right)g(a)\mathrm{d}a}{k(\tan^2\omega+1)\sqrt{\frac{k^2(\tan^2\omega+1)}{\tan^2\omega+k^2}a^2 - l^2}}\int_0^{2\pi}\int_0^\pi \cos\psi f(\alpha,\beta)\mathrm{d}\alpha\mathrm{d}\beta \tag{21}$$

Combining Eqs. (10) and (21), N_l can be rewritten as

$$N_l = \frac{l\mathrm{d}l}{\tau\mu_a}\int_0^1 g(k)\mathrm{d}k\int_0^\pi g(\omega)\mathrm{d}\omega\cdot \int_{l\Big/\sqrt{\frac{k^2(\tan^2\omega+1)}{\tan^2\omega+k^2}}}^{+\infty} \frac{\left(\tan^2\omega+k^2\right)g(a)\mathrm{d}a}{k(\tan^2\omega+1)\sqrt{\frac{k^2(\tan^2\omega+1)}{\tan^2\omega+k^2}a^2 - l^2}} \tag{22}$$

Hence, the PDF $f(l)$ of trace length l can be obtained by

$$f(l) = \frac{l}{\tau\mu_a}\int_0^1 g(k)\mathrm{d}k\int_0^\pi g(\omega)\mathrm{d}\omega \int_{l\Big/\sqrt{\frac{k^2(\tan^2\omega+1)}{\tan^2\omega+k^2}}}^{+\infty} \frac{\left(\tan^2\omega+k^2\right)g(a)\mathrm{d}a}{k(\tan^2\omega+1)\sqrt{\frac{k^2(\tan^2\omega+1)}{\tan^2\omega+k^2}a^2 - l^2}} \quad \left(l \le \sqrt{\frac{k^2(\tan^2\omega+1)}{\tan^2\omega+k^2}}a\right) \tag{23}$$

Note that when k and ω are constant, Eq. (23) can be simplified as

$$f(l) = \frac{l}{\sqrt{\frac{k^2(\tan^2\omega+1)}{\tan^2\omega+k^2}}\mu_a} \int_{l\Big/\sqrt{\frac{k^2(\tan^2\omega+1)}{\tan^2\omega+k^2}}}^{+\infty} \frac{g(a)\mathrm{d}a}{\sqrt{\frac{k^2(\tan^2\omega+1)}{\tan^2\omega+k^2}a^2 - l^2}} \quad \left(l \le \sqrt{\frac{k^2(\tan^2\omega+1)}{\tan^2\omega+k^2}}a\right) \tag{24}$$

This is consistent with that derived by Zhang et al. (2002) when k is also defined as the ratio of short-long axis lengths.

According to the PDF of trace line l, the mth moment of the trace length of $E(l)$ can be expressed as

$$E(l^m) = \int_0^{+\infty} l^m f(l)\mathrm{d}l \tag{25}$$

where $E(\cdot)$ represents the expected value of the function within the parentheses.

Combining Eqs. (23) and (25), we can obtain

$$E(l^m) = \frac{1}{\tau\mu_a}\int_0^{+\infty} l^m\mathrm{d}l\int_0^1 g(k)\mathrm{d}k\int_0^\pi g(\omega)\mathrm{d}\omega\cdot \int_{l\Big/\sqrt{\frac{k^2(\tan^2\omega+1)}{\tan^2\omega+k^2}}}^{+\infty} \frac{\left(\tan^2\omega+k^2\right)lg(a)\mathrm{d}a}{k(\tan^2\omega+1)\sqrt{\frac{k^2(\tan^2\omega+1)}{\tan^2\omega+k^2}a^2 - l^2}} \tag{26}$$

Reversing the order of integration in Eq. (26) and integrating over l gives

$$E(l^m)=\frac{1}{\tau\mu_a}\int_0^{+\infty}g(a)\mathrm{d}a\int_0^1 g(k)\mathrm{d}k\int_0^{\pi}g(\omega)\mathrm{d}\omega\int_0^{\sqrt{\frac{k^2(\tan^2\omega+1)}{\tan^2\omega+k^2}}a}\frac{\left(\tan^2\omega+k^2\right)l^{m+1}\mathrm{d}l}{k(\tan^2\omega+1)\sqrt{\frac{k^2(\tan^2\omega+1)}{\tan^2\omega+k^2}a^2-l^2}}=\frac{J_{m+1}}{\tau\mu_a}\int_0^{+\infty}a^{m+1}g(a)\mathrm{d}a\cdot\int_0^1\int_0^{\pi}k^m\left(\sqrt{\frac{\tan^2\omega+1}{\tan^2\omega+k^2}}\right)^{m-1}g(k)g(\omega)\mathrm{d}k\mathrm{d}\omega \tag{27}$$

where

$$J_{m+1}=\begin{cases}\dfrac{1\times3\times\cdots\times m}{2\times4\times\cdots\times(m+1)}\dfrac{\pi}{2} & (m\text{ is odd})\\ \dfrac{2\times4\times\cdots\times m}{3\times5\times\cdots\times(m+1)} & (m\text{ is even})\end{cases} \tag{28}$$

Furthermore, the $(m+1)$th moment of a can be given by

$$E\left(a^{m+1}\right)=\int_0^{+\infty}a^{m+1}g(a)\mathrm{d}a \tag{29}$$

Hence, Eq. (27) can be further expressed as

$$E(l^m)=\frac{J_{m+1}}{\tau\mu_a}E\left(a^{m+1}\right)\int_0^1\int_0^{\pi}k^m\left(\sqrt{\frac{\tan^2\omega+1}{\tan^2\omega+k^2}}\right)^{m-1}\cdot g(k)g(\omega)\mathrm{d}k\mathrm{d}\omega \tag{30}$$

For $m=1$ and $m=2$, we can obtain

$$E(l)=\frac{\pi E(a^2)E(k)}{4\tau\mu_a} \tag{31}$$

$$E\left(l^2\right)=\frac{2E(a^3)}{3\tau\mu_a}\int_0^1\int_0^{\pi}k^2\sqrt{\frac{\tan^2\omega+1}{\tan^2\omega+k^2}}g(k)g(\omega)\mathrm{d}k\mathrm{d}\omega \tag{32}$$

where

$$E(k)=\int_0^1 kg(k)\mathrm{d}k \tag{33}$$

The mean value and standard deviation of the trace length, the mean value and standard deviation of the length of the long axis can be denoted as μ_l, σ_l, μ_a and σ_a, respectively. Substituting $E(l)=\mu_l$, $E(l^2)=\mu_l^2+\sigma_l^2$, $E(a^2)=\mu_a^2+\sigma_a^2$ into Eqs. (31) and (32), μ_l and σ_l^2 can be expressed as

$$\mu_l=\frac{\pi(\mu_a{}^2+\sigma_a^2)E(k)}{4\tau\mu_a} \tag{34}$$

$$\sigma_l^2=\frac{2E(a^3)}{3\tau\mu_a}\int_0^1\int_0^{\pi}k^2\sqrt{\frac{\tan^2\omega+1}{\tan^2\omega+k^2}}g(k)g(\omega)\mathrm{d}k\mathrm{d}\omega-\frac{\pi^2\left(\mu_a^2+\sigma_a^2\right)^2\mu_k^2}{16\tau^2\mu_a^2} \tag{35}$$

where μ_l and σ_l are the mean value and standard deviation of the trace length, respectively; and σ_a is the standard deviation of the length of the long axis.

The expressions of ω (the angle between the long axis line and trace line) and $g(\omega)$ are essential to the calculation of μ_l and σ_l^2. The derivation of ω and $g(\omega)$ can be found in Appendix A. For simplicity,

Table 3
The orientation (δs/θs) of the sampling windows (SW).

SW No.	δ_s (°)/θ_s (°)	SW No.	δ_s (°)/θ_s (°)
1	15/0	16	15/180
2	30/0	17	30/180
3	45/0	18	45/180
4	60/0	19	60/180
5	75/0	20	75/180
6	15/60	21	15/240
7	30/60	22	30/240
8	45/60	23	45/240
9	60/60	24	60/240
10	75/60	25	75/240
11	15/120	26	15/300
12	30/120	27	30/300
13	45/120	28	45/300
14	60/120	29	60/300
15	75/120	30	75/300

Table 2
The geometric characteristics of the UED model.

Geometric characteristic	Geometric parameter	Distribution form	Distribution parameter
Central point	Location 3D Density P_{30} (m^{-3})	Poisson distribution	2
Size	Length of the long axis (m)	Gamma distribution	Shape parameter: 1.5; Inverse scale parameter: 0.5
	Ratio of short-long axis lengths	Normal distribution	Mean value = 0.5; Standard deviation = 0.1
Azimuth	Orientation	Fisher distribution	Mean dip direction = 300°; Mean dip angle = 55°; Fisher constant: 15
	Rotation angle	Von Mises distribution	Mean rotation angle: 30°; Von Mises constant: 15

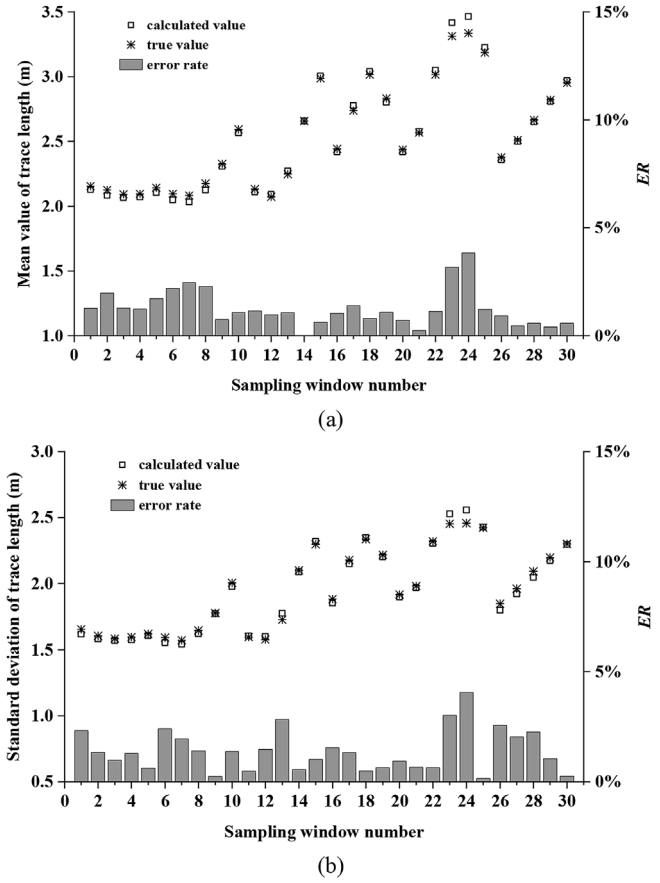

Fig. 5. The mean value and standard deviation of trace length and the *ER*s in 30 sampling windows: (a) Mean trace length, and (b) Standard deviation of trace length.

$\omega(\alpha, \beta, \gamma, \beta_s, \alpha_s)$ is used to represent the complex expression of ω. Hence, μ_l and σ_l^2 can be rewritten as

$$\mu_l = \frac{\pi(\mu_a^2 + \sigma_a^2)E(k)}{4\tau\mu_a} \tag{36}$$

$$\sigma_l^2 = \frac{2\eta E(a^3)}{3\tau\mu_a} - \mu_l^2 \tag{37}$$

where

$$\tau = \int_0^{2\pi}\int_0^{\pi}\int_{-\pi/2}^{\pi/2}\int_0^1 \sqrt{\frac{\tan^2[\omega(\alpha,\beta,\gamma,\alpha_s,\beta_s)]+k^2}{\tan^2[\omega(\alpha,\beta,\gamma,\alpha_s,\beta_s)]+1}} f(\alpha,\beta)\cdot \mathrm{d}\alpha\mathrm{d}\beta f(\gamma)\mathrm{d}\gamma g(k)\mathrm{d}k \tag{38}$$

$$\eta = \int_0^{2\pi}\int_0^{\pi}\int_{-\pi/2}^{\pi/2}\int_0^1 k^2\sqrt{\frac{\tan^2[\omega(\alpha,\beta,\gamma,\alpha_s,\beta_s)]+1}{\tan^2[\omega(\alpha,\beta,\gamma,\alpha_s,\beta_s)]+k^2}} f(\alpha,\beta)\cdot \mathrm{d}\alpha\mathrm{d}\beta f(\gamma)\mathrm{d}\gamma g(k)\mathrm{d}k \tag{39}$$

3.2. Validation by Monte Carlo simulation

In order to validate Eqs. (36) and (37), a set of hypothetical 3D elliptical DFN was constructed in a block based on Monte Carlo simulation. The geometric characteristics of the UED model are listed in Table 2. The block size is 50 m × 50 m × 50 m (length × width × height), and 250,000 elliptical fractures were generated in the block.

Table 4
The known and unknown parameters in the parameter estimation of the UED model.

Characteristic parameter	Statistical parameter	State
Orientation of the sampling window	α_s, β_s	Known
Trace length	μ_l, σ_l	Known
Orientation of fractures in UED	α_m, β_m, κ_1	Known
Length of the long axis in UED	μ_a, σ_a	Unknown
Ratio of short-long axis lengths in UED	μ_k, σ_k	Unknown
Rotation angle in UED	κ_2, γ_m	Unknown

Thirty infinite sampling windows were used to collect the trace information. The orientations are listed in Table 3. The mean value and standard deviation of the trace length by Monte Carlo simulation were viewed as the true values. The calculated values of the mean and standard deviation of the trace length are calculated by Eqs. (36) and (37).

In order to compare the differences between the true and calculated values, the error rate (*ER*) is defined as

$$ER = \frac{|TV - CV|}{TV} \times 100\% \tag{40}$$

where *TV* is the true value of the mean value or standard deviation of the trace length; and *CV* is the calculated value of the mean value or standard deviation of the trace length based on Eqs. (36) and (37).

The calculated and true values of the mean trace length and their *ER*s are shown in Fig. 5a, while the calculated and true values of the standard deviation of mean trace lengths and their *ER*s are shown in Fig. 5b. The results show that the calculated values are in good agreement with the true ones, and the *ER*s of the mean value and standard deviation of trace length are less than 5%. The good match between the true and calculated values verified the correctness of Eqs. (36) and (37).

4. Estimation of the size- and azimuth-related parameters in the UED model based on the trace length

According to the above-mentioned derivation, the distribution of trace length depends on the distributions of the length of the long axis, ratio of short-long axis lengths, orientation and rotation angle. It is not easy to obtain distributions of the size and azimuth in the UED model via the trace information only. With respect to the size inference of the non-UED model, Zhang et al. (2002) inferred the fracture size distribution from the trace length distribution by assuming that the length of the long axis obeys certain distributions including log-normal distribution, negative exponential and gamma distributions. Jin et al. (2014) built up the relationship between the size and trace distributions by assuming that the trace length obeys certain distributions including uniform, fractal, exponential, and polynomial distributions. In this paper, we first assume that the length of the long axis, ratio of short-long axis lengths, orientation, and rotation angle obey certain distribution patterns, and then estimate the corresponding statistical parameters based on the trace information from multiple sampling windows.

4.1. Assumption of size and azimuth distributions

The PDF that can describe the fracture orientations includes Fisher distribution (Zheng et al., 2014b), Bingham distribution

(Bingham, 1974), and Bivariate normal distribution (Kulatilake, 1986). Among these distributions, the Fisher distribution is the most commonly used one since it only has one parameter (Fisher et al., 1987). Its general PDF is defined as

$$f(\beta,\alpha)=\frac{\kappa_1 \sin\beta e^{\kappa_1[\sin\beta \sin\beta_m \cos(\alpha-\alpha_m)+\cos\beta \cos\beta_m]}}{4\pi\sinh\kappa_1} \tag{41}$$

where κ_1 is a parameter quantifying the degree of clustering; and β_m and α_m are the location parameters. In this study, the Fisher distribution is adopted to describe the orientation of fractures. For one rock mass, the values of β_m, α_m and κ_1 can be estimated according to the plunge and trend of the trace (Kemey and Post, 2003).

As fractures are the product of geological tectonic movement, its propagation may follow a preferred direction in a homogeneous region of the rock mass, which is related to the direction of the long axis of the elliptical fracture. According to this property, the rotation angle would tend to align with a preferred direction, and the direction of the long axis can be described by the von Mises distribution (Zheng et al., 2022) as

$$f(\gamma)=C^{-1}e^{\kappa_2 \cos(\gamma-\gamma_m)} \quad (0\le\gamma\le 2\pi) \tag{42a}$$

$$C=2\pi I_0(\kappa_2) \tag{42b}$$

$$I_0(\kappa_2)=1+\frac{\left(\frac{\kappa_2}{2}\right)^2}{1!^2}+\frac{\left(\frac{\kappa_2}{2}\right)^4}{2!^2}+\frac{\left(\frac{\kappa_2}{2}\right)^6}{3!^2}+\cdots \tag{42c}$$

where γ_m is the location parameter, κ_2 is the concentration parameter, and C is a code without practical significance.

For the rotation angle ranging from $-\pi/2$ to $\pi/2$, the von Mises distribution pattern needs to be used in a truncated form. In other words, the variable γ is truncated as in the range of $-\pi/2\le\gamma-\gamma_m\le\pi/2$, and the probability functions are corrected with a normalizing coefficient of C_1, which can be calculated by

$$\int_{\gamma_m-\pi/2}^{\gamma_m+\pi/2} C_1^{-1}e^{\kappa_2 \cos(\gamma-\gamma_m)}=1 \tag{43a}$$

$$C_1=\pi I_0(\kappa_2)+I_1(\kappa_2) \tag{43b}$$

$$I_1(\kappa_2)=(2\kappa_2)+\frac{1!^2(2\kappa_2)^3}{3!^2}+\frac{2!^2(2\kappa_2)^5}{5!^2}+\frac{3!^2(2\kappa_2)^7}{7!^2}+\cdots \tag{43c}$$

Furthermore, numerical tests show that when κ_2 is larger than 6, the value of C_1 is close to that of C. This means that Eq. (42) can be directly used to describe the distribution of rotation angle without correcting the coefficient C.

For the size distribution, the length of the long axis may follow the negative exponential distribution, log-normal distribution, and gamma distribution. The ratio of short-long axis lengths may follow the uniform distribution, normal distribution, gamma distribution. Since the range of the ratio of short-long axis lengths ranges from 0 to 1, it can be characterized by truncated forms. We assume the length of the long axis to be in the negative exponential distribution and the ratio of short-long axis lengths in the normal distribution to illustrate the process of parameter estimation. The PDF of the ratio of short-long axis lengths can be given by

$$g(k)=\frac{1}{\sqrt{2\pi}\sigma_k}\exp\left[-\frac{(k-\mu_k)^2}{2\sigma_k^2}\right] \tag{44}$$

where μ_k and σ_k are the mean value and standard deviation of k, respectively.

According to the above distribution assumptions, τ and η, $E(k)$ can be rewritten as

$$\tau=\int_0^{2\pi}\int_0^{\pi}\int_{-\frac{\pi}{2}+\gamma_m}^{\frac{\pi}{2}+\gamma_m}\int_0^1 \frac{\sqrt{\tan^2[\omega(\alpha,\beta,\gamma,\alpha_s,\beta_s)]+k^2}}{\sqrt{\tan^2[\omega(\alpha,\beta,\gamma,\alpha_s,\beta_s)]+1}}\cdot \frac{\kappa_1 \sin\beta e^{\kappa_1(\sin\beta \sin\beta_m \cos(\alpha-\alpha_m)+\cos\beta \cos\beta_m)}}{4\pi\sinh\kappa_1}\frac{e^{\kappa_2 \cos(\gamma-\gamma_m)}}{\pi I_0(\kappa_2)+I_1(\kappa_2)}\frac{1}{\sqrt{2\pi}\sigma_k}\cdot \exp\left[-\frac{(k-\mu_k)^2}{2\sigma_k^2}\right]\mathrm{d}\alpha\mathrm{d}\beta\mathrm{d}\gamma\mathrm{d}k \tag{45}$$

$$\eta=\int_0^{2\pi}\int_0^{\pi}\int_{-\frac{\pi}{2}+\gamma_m}^{\frac{\pi}{2}+\gamma_m}\int_0^1 k^2\frac{\sqrt{\tan^2[\omega(\alpha,\beta,\gamma,\alpha_s,\beta_s)]+1}}{\sqrt{\tan^2[\omega(\alpha,\beta,\gamma,\alpha_s,\beta_s)]+k^2}}\cdot \frac{\kappa_1 \sin\beta e^{\kappa_1[\sin\beta \sin\beta_m \cos(\alpha-\alpha_m)+\cos\beta \cos\beta_m]}}{4\pi\sinh\kappa_1}\frac{e^{\kappa_2 \cos(\gamma-\gamma_m)}}{\pi I_0(\kappa_2)+I_1(\kappa_2)}\frac{1}{\sqrt{2\pi}\sigma_k}\cdot \exp\left[-\frac{(k-\mu_k)^2}{2\sigma_k^2}\right]\mathrm{d}\alpha\mathrm{d}\beta\mathrm{d}\gamma\mathrm{d}k \tag{46}$$

$$E(k)=\int_0^1 \frac{1}{\sqrt{2\pi}\sigma_k}\exp\left[-\frac{(k-\mu_k)^2}{2\sigma_k^2}\right]\mathrm{d}k \tag{47}$$

It should be noted that k ranges from 0 to 1, and $E(k)$ is not necessarily equal to the mean value of k.

Eqs. (45)-(47) are the expressions of τ and η, $E(k)$ of the trace length of the UED model whose parameters can be given as a specific distribution on one sampling window. All related parameters are summarized in Table 4. As shown in the table, six unknown parameters, i.e. γ_m, κ_2, μ_a, σ_a, μ_k, σ_k, should be estimated. At least three sampling windows are required to estimate these parameters according to the number of unknown parameters.

Eqs. (45) and (46) are complex, and it is difficult to derive an analytical solution. Therefore, Monte Carlo simulation is proposed to solve the integral (Evans and Swartz, 2000). The basic principle can be found in Appendix B. Hence, the approximate values of τ and η in Eqs. (45) and (46), which are labeled as τ_j and η_j under one sampling window of j, respectively, can be given by

$$\overline{\tau_j}=\frac{2\pi^3}{N}\sum_{i=1}^{N}\frac{\sqrt{\tan^2\left[\omega\left(\alpha_i,\beta_i,\gamma_i,\alpha_{sj},\beta_{sj}\right)\right]+k_i^2}}{\sqrt{\tan^2\left[\omega\left(\alpha_i,\beta_i,\gamma_i,\alpha_{sj},\beta_{sj}\right)\right]+1}}\cdot \frac{\kappa_1 \sin\beta_i e^{\kappa_1(\sin\beta_i \sin\beta_m \cos(\alpha_i-\alpha_m)+\cos\beta_i \cos\beta_m)}}{4\pi\sinh\kappa_1}\frac{e^{\kappa_2 \cos[2(\gamma_i-\gamma_m)]}}{2\pi I_0(\kappa_2)}\frac{1}{\sqrt{2\pi}\sigma_k}\cdot \exp\left[-\frac{(k_i-\mu_k)^2}{2\sigma_k^2}\right] \tag{48}$$

$$\overline{\eta_j}=\frac{2\pi^3}{N}\sum_{i=1}^{N}k_i^2\frac{\sqrt{\tan^2\left[\omega\left(\alpha_i,\beta_i,\gamma_i,\alpha_{sj},\beta_{sj}\right)\right]+1}}{\sqrt{\tan^2\left[\omega\left(\alpha_i,\beta_i,\gamma_i,\alpha_{sj},\beta_{sj}\right)\right]+k_i^2}}\cdot \frac{\kappa_1\sin\beta_i e^{\kappa_1[\sin\beta_i\sin\beta_m\cos(\alpha_i-\alpha_m)+\cos\beta_i\cos\beta_m]}}{4\pi\sinh\kappa_1}\frac{e^{\kappa_2\cos[2(\gamma_i-\gamma_m)]}}{2\pi I_0(\kappa_2)}\frac{1}{\sqrt{2\pi}\sigma_k}\cdot \exp\left[-\frac{(k_i-\mu_k)^2}{2\sigma_k^2}\right] \tag{49}$$

where N is the total number of the random number sequence generated by Monte Calo simulation; α_{sj} and β_{sj} are the dip direction and dip angle of sampling window j, respectively; α_i, β_i, γ_i and k_i are the ith random dip direction, dip angle, rotation angle, and ratio of the short-long axis lengths, respectively, and their ranges are $0\le\alpha_i\le 2\pi$, $0\le\beta_i\le\pi$, $-\pi\le\gamma_i\le\pi$ and $0<k_i\le 1$, respectively.

4.2. Estimate parameters by optimization algorithm

According to the number of unknown parameters, at least three sampling windows are required. Thus, this paper uses the following example to show the process of parameter estimation. The mean value and standard deviation of the trace length based on Eqs. (36) and (37) can be given by

$$\left.\begin{aligned}\mu_{l1}&=\frac{\pi(\mu_a^2+\sigma_a^2)E(k)}{4\tau_1\mu_a}\\ \mu_{l2}&=\frac{\pi(\mu_a^2+\sigma_a^2)E(k)}{4\tau_2\mu_a}\\ \mu_{l3}&=\frac{\pi(\mu_a^2+\sigma_a^2)E(k)}{4\tau_3\mu_a}\end{aligned}\right\} \tag{50}$$

$$\left.\begin{aligned}\sigma_{l1}^2&=\frac{2\eta_1E\left(a^3\right)}{3\tau_1\mu_a}-\mu_{l1}^2\\ \sigma_{l2}^2&=\frac{2\eta_2E\left(a^3\right)}{3\tau_2\mu_a}-\mu_{l2}^2\\ \sigma_{l3}^2&=\frac{2\eta_3E\left(a^3\right)}{3\tau_3\mu_a}-\mu_{l3}^2\end{aligned}\right\} \tag{51}$$

where μ_{l1}, σ_{l1}, τ_1 and η_1 are obtained from Sampling Window 1; μ_{l2}, σ_{l2}, τ_2 and η_2 are obtained from Sampling Window 2; and μ_{l3}, σ_{l3}, τ_3 and η_3 are obtained from Sampling Window 3.

Obviously, the difference in the mean value and standard deviation of the trace length between sampling windows depends mainly on the differences of τ and η. To simplify these equations, the combination of any two of the three sampling windows can eliminate some common unknown parameters, and hence Eqs. (50) and (51) can be rearranged as

$$\left.\begin{aligned}\frac{\mu_{l1}}{\mu_{l2}}&=\frac{\tau_2}{\tau_1}\\ \frac{\mu_{l1}}{\mu_{l3}}&=\frac{\tau_3}{\tau_1}\\ \frac{\mu_{l2}}{\mu_{l3}}&=\frac{\tau_3}{\tau_2}\end{aligned}\right\} \tag{52}$$

$$\left.\begin{aligned}\frac{\sigma_{l1}^2+\mu_{l1}^2}{\sigma_{l2}^2+\mu_{l2}^2}\frac{\tau_1}{\tau_2}&=\frac{\eta_1}{\eta_2}\\ \frac{\sigma_{l1}^2+\mu_{l1}^2}{\sigma_{l3}^2+\mu_{l3}^2}\frac{\tau_1}{\tau_3}&=\frac{\eta_1}{\eta_3}\\ \frac{\sigma_{l2}^2+\mu_{l2}^2}{\sigma_{l3}^2+\mu_{l3}^2}\frac{\tau_2}{\tau_3}&=\frac{\eta_2}{\eta_3}\end{aligned}\right\} \tag{53}$$

Substituting Eq. (52) into Eq. (53), we can obtain

$$\left.\begin{aligned}\frac{\sigma_{l1}^2+\mu_{l1}^2}{\sigma_{l2}^2+\mu_{l2}^2}\frac{\mu_{l2}}{\mu_{l1}}&=\frac{\eta_1}{\eta_2}\\ \frac{\sigma_{l1}^2+\mu_{l1}^2}{\sigma_{l3}^2+\mu_{l3}^2}\frac{\mu_{l3}}{\mu_{l1}}&=\frac{\eta_1}{\eta_3}\\ \frac{\sigma_{l2}^2+\mu_{l2}^2}{\sigma_{l3}^2+\mu_{l3}^2}\frac{\mu_{l3}}{\mu_{l2}}&=\frac{\eta_2}{\eta_3}\end{aligned}\right\} \tag{54}$$

Eqs. (52) and (54) are the corresponding relationship between the trace length, τ and η of the three sampling windows. Combining with the Monte Carlo integrals in Eqs. (48) and (49), Eqs. (52) and (54) can be rewritten as

$$\left.\begin{aligned}\frac{\overline{\tau_2}}{\overline{\tau_1}}&\approx\frac{\mu_{l1}}{\mu_{l2}}\\ \frac{\overline{\tau_3}}{\overline{\tau_1}}&\approx\frac{\mu_{l1}}{\mu_{l3}}\\ \frac{\overline{\tau_3}}{\overline{\tau_2}}&\approx\frac{\mu_{l2}}{\mu_{l3}}\end{aligned}\right\} \tag{55}$$

$$\left.\begin{aligned}\frac{\overline{\eta_1}}{\overline{\eta_2}}&\approx\frac{\sigma_{l1}^2+\mu_{l1}^2}{\sigma_{l2}^2+\mu_{l2}^2}\frac{\mu_{l2}}{\mu_{l1}}\\ \frac{\overline{\eta_1}}{\overline{\eta_3}}&\approx\frac{\sigma_{l1}^2+\mu_{l1}^2}{\sigma_{l3}^2+\mu_{l3}^2}\frac{\mu_{l3}}{\mu_{l1}}\\ \frac{\overline{\eta_2}}{\overline{\eta_3}}&\approx\frac{\sigma_{l2}^2+\mu_{l2}^2}{\sigma_{l3}^2+\mu_{l3}^2}\frac{\mu_{l3}}{\mu_{l2}}\end{aligned}\right\} \tag{56}$$

where $\overline{\tau_1}$, $\overline{\eta_1}$, $\overline{\tau_2}$, $\overline{\eta_2}$, $\overline{\tau_3}$ and $\overline{\eta_3}$ are the Monte Carlo integrals of τ_1, η_1, τ_2, η_2, τ_3 and η_3, respectively.

It is still difficult to solve Eqs. (55) and (56) directly, hence we estimate the parameters by constructing the optimization function. For the parameters μ_{l1}, σ_{l1}, μ_{l2}, σ_{l2}, τ_1, η_1, τ_2 and η_2 from the Sampling Windows 1 and 2, the following inequality equations can be obtained based on Eqs. (55) and (56):

$$\left.\begin{aligned}&\left|\frac{\overline{\tau_2}}{\overline{\tau_1}}-\frac{\mu_{l1}}{\mu_{l2}}\right|\ge 0\\ &\left|\frac{\overline{\eta_1}}{\overline{\eta_2}}-\frac{\sigma_{l1}^2+\mu_{l1}^2}{\sigma_{l2}^2+\mu_{l2}^2}\frac{\mu_{l2}}{\mu_{l1}}\right|\ge 0\end{aligned}\right\} \tag{57}$$

$$\left.\begin{aligned}&|\overline{\tau_1}\mu_{l1}-\overline{\tau_2}\mu_{l2}|\ge 0\\ &\left|\overline{\eta_2}\mu_{l2}\left(\sigma_{l1}^2+\mu_{l1}^2\right)-\overline{\eta_1}\mu_{l1}\left(\sigma_{l2}^2+\mu_{l2}^2\right)\right|\ge 0\end{aligned}\right\} \tag{58}$$

According to Eqs. (57) and (58), two optimization functions $E_{12(1)}$ and $E_{12(2)}$ can be formulated as

$$\left.\begin{aligned} E_{12(1)} &= \left|\frac{\overline{\tau_2}}{\overline{\tau_1}}-\frac{\mu_{l1}}{\mu_{l2}}\right|+\left|\frac{\overline{\eta_1}}{\overline{\eta_2}}-\frac{\sigma_{l1}^2+\mu_{l1}^2}{\sigma_{l2}^2+\mu_{l2}^2}\frac{\mu_{l2}}{\mu_{l1}}\right| \\ E_{12(2)} &= \left|\overline{\tau_1}\mu_{l1}-\overline{\tau_2}\mu_{l2}\right|+\left|\overline{\eta_2}\mu_{l2}\left(\sigma_{l1}^2+\mu_{l1}^2\right)-\overline{\eta_1}\mu_{l1}\left(\sigma_{l2}^2+\mu_{l2}^2\right)\right| \end{aligned}\right\} \tag{59}$$

Hence, the estimations of μ_k, σ_k, γ_m and κ_2 are a problem of solving the minimum value of the optimization functions. Combined with the trace information in Sampling Window 3, the optimization functions can be given by

$$\left.\begin{aligned} E_{12(1)} &= \left|\frac{\overline{\tau_2}}{\overline{\tau_1}}-\frac{\mu_{l1}}{\mu_{l2}}\right|+\left|\frac{\overline{\eta_1}}{\overline{\eta_2}}-\frac{\sigma_{l1}^2+\mu_{l1}^2}{\sigma_{l2}^2+\mu_{l2}^2}\frac{\mu_{l2}}{\mu_{l1}}\right| \\ E_{12(2)} &= \left|\overline{\tau_1}\mu_{l1}-\overline{\tau_2}\mu_{l2}\right|+\left|\overline{\eta_2}\mu_{l2}\left(\sigma_{l1}^2+\mu_{l1}^2\right)-\overline{\eta_1}\mu_{l}\left(\sigma_{l2}^2+\mu_{l2}^2\right)\right| \\ E_{13(1)} &= \left|\frac{\overline{\tau_3}}{\overline{\tau_1}}-\frac{\mu_{l1}}{\mu_{l3}}\right|+\left|\frac{\overline{\eta_1}}{\overline{\eta_3}}-\frac{\sigma_{l1}^2+\mu_{l1}^2}{\sigma_{l3}^2+\mu_{l3}^2}\frac{\mu_{l3}}{\mu_{l1}}\right| \\ E_{13(2)} &= \left|\overline{\tau_1}\mu_{l1}-\overline{\tau_3}\mu_{l3}\right|+\left|\overline{\eta_3}\mu_{l3}\left(\sigma_{l1}^2+\mu_{l1}^2\right)-\overline{\eta_1}\mu_{l1}\left(\sigma_{l3}^2+\mu_{l3}^2\right)\right| \\ E_{23(1)} &= \left|\frac{\overline{\tau_3}}{\overline{\tau_2}}-\frac{\mu_{l2}}{\mu_{l3}}\right|+\left|\frac{\overline{\eta_2}}{\overline{\eta_3}}-\frac{\sigma_{l2}^2+\mu_{l2}^2}{\sigma_{l3}^2+\mu_{l3}^2}\frac{\mu_{l3}}{\mu_{l2}}\right| \\ E_{23(2)} &= \left|\overline{\tau_2}\mu_{l2}-\overline{\tau_3}\mu_{l3}\right|+\left|\overline{\eta_3}\mu_{l3}\left(\sigma_{l2}^2+\mu_{l2}^2\right)-\overline{\eta_2}\mu_{l2}\left(\sigma_{l3}^2+\mu_{l3}^2\right)\right| \end{aligned}\right\} \tag{60}$$

where $E_{ij(p)}$ represents the optimization function p constructed by the Sampling Windows i and j. Each optimization function represents an objective equation, and all objective equations are combined to estimate the parameters. It should be noted that multiple sets of optimization results can be obtained for the solving process. When a set of estimated parameters of μ_k, σ_k, γ_m, κ_2 minimize the sum E_{sum}, the result of μ_k, σ_k, γ_m, κ_2 is the best-estimated value, where E_{sum} is defined as

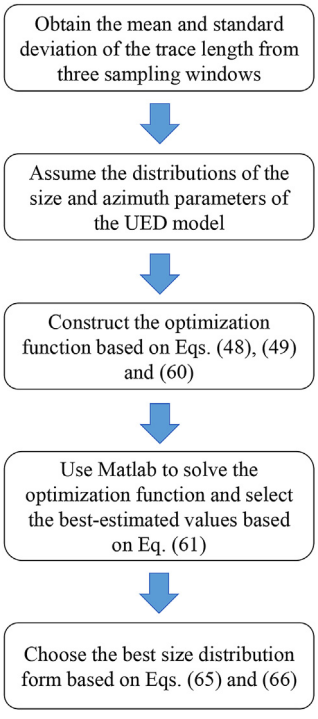

Fig. 6. Flowchart of estimating the size- and azimuth-related parameters of the UED model.

Table 5
The parameters and distributions of the characteristics of the UED model.

Characteristic	Orientation	Rotation angle	Short-long axis length ratio	Long axis length
Distribution form	Fisher distribution	Von Mises distribution	Normal distribution	Exponential distribution
Parameter	$\kappa_1 = 15$; $\alpha_m = 60°$; $\beta_m = 150°$	$\kappa_2 = 20$; $\gamma_m = 60°$	$\mu_k = 0.4$; $\sigma_k = 0.2$	$\mu_a = 2$; $\sigma_a = 2$

$$E_{sum} = E_1 + E_2 + E_3 + E_4 + E_5 + E_6 \tag{61}$$

Based on the assumption that the length of the long axis follows an exponential distribution, μ_a and σ_a can be obtained by

$$\mu_a = \sigma_a = \frac{2\tau\mu_l}{\pi E(k)} \tag{62}$$

τ, η and $E(k)$ can be calculated according to Eqs. (45)-(47). For other distribution patterns of fracture size and azimuth, the methodology as described above can also be valid.

With respect to one set of fractures, the mean value and standard deviation of trace length in each sampling window are determined. If the assumed distributions of the length of the long axis, ratio of short-long axis lengths are different, we may obtain different values of μ_a, σ_a, μ_k, σ_k based on the trace information. In order to keep uniqueness, similar to Zhang et al. (2002)'s method, the third moment of the trace length distribution is used to verify the suitability of the assumed size distribution pattern. According to Eq. (30), $E(l^3)$ can be expressed as

$$E\left(l^3\right) = \frac{3\pi}{16\tau E(a)}E\left(a^4\right)\rho \tag{63}$$

where ρ is defined as

$$\rho = \int_0^{2\pi}\int_0^{\pi}\int_{-\pi/2+\gamma_m}^{\pi/2+\gamma_m}\int_0^1 k^3\frac{\tan^2[\omega(\alpha,\beta,\gamma,\alpha_s,\beta_s)]+1}{\tan^2[\omega(\alpha,\beta,\gamma,\alpha_s,\beta_s)]+k^2} f(\alpha,\beta)\mathrm{d}\alpha\mathrm{d}\beta f(\gamma)\mathrm{d}\gamma g(k)\mathrm{d}k \tag{64}$$

The distributions of the ratio of short-long axis lengths can be verified by the trace lengths in two different sampling windows as

$$\frac{\rho_1\tau_2}{\rho_2\tau_1} = \frac{E_1\left(l^3\right)}{E_2\left(l^3\right)} \tag{65}$$

When the distribution of the ratio of short-long axis lengths is determined, the distribution of the length of the long axis can be verified by

Table 6
The mean value and standard deviation of trace length in the three combinations of sampling windows.

δ_s (°)/θ_s (°) of sampling windows	Mean value	Standard deviation
30/0	1.7006	1.6115
60/30	1.3528	1.3179
45/120	1.4451	1.4162

Table 7
The estimated values of μ_a, σ_a, μ_k, σ_k, γ_m, κ_2 in different combinations of the sampling windows with different orientations.

Orientation in three combinations (δ_s (°)/θ_s (°))	Rotation angle		Ratio of short-long axis lengths		Length of the long axis	
	κ_2	γ_m	μ_k	σ_k	μ_a	σ_a
30/0, 60/30, 45/120	22.3	60.3°	0.409	0.205	1.97	1.97
15/240, 30/240, 60/240	21.5	60.2°	0.398	0.196	2.02	2.02
75/150, 75/210, 75/300	21.7	59.8°	0.402	0.204	1.98	1.98
True value	20	60°	0.4	0.2	2	2
Mean error rate	9.17%	0.17%	0.75%	0.83%	0.5%	0.5%

$$\frac{E(a^4)}{E(a)} = \frac{16\tau E\left(l^3\right)}{3\pi\rho} \tag{66}$$

Fig. 6 summarizes the procedures of estimating the size- and azimuth-related parameters in the UED model.

5. Model validation and application

In order to validate the above-mentioned estimation method, a hypothetical case study is performed, and the parameters and distributions of the UED model are shown in Table 5. The rock block size is assumed to be 50 m × 50 m × 50 m (length × width × height), with a 3D density of 2 m^{-3}, and 250,000 elliptical fractures. Firstly, the mean value and standard deviation of the trace length in one sampling window are obtained. Then, the parameters are deduced based on the trace information. The parameters to be estimated include the mean μ_a and standard deviation σ_a of the length of the long axis, mean μ_k and standard deviation σ_k of the ratio of short-long axis lengths, and location parameter γ_m and concentration degree κ_2 of the rotation angle.

To verify the generality of parameter estimation, three combinations of sampling windows with different orientations have been used: (1) the dip angles and dip directions of the three sampling windows are different; (2) the dip directions of the three sampling windows are the same, while the dip angles are different; and (3) the dip angles of the three sampling windows are the same, while the dip directions are different. The first combination is taken as an example to illustrate the application of parameter estimation.

The orientations of the first combination and the corresponding mean value and standard deviation of trace length are shown in Table 6. The right side of Eqs. (55) and (56) can be easily computed based on the mean value and standard deviation of the trace length in Table 6. The left side of Eqs. (55) and (56) can be obtained by Eqs. (48) and (49), respectively, combining the Monte Carlo simulation. The final optimization function can be obtained by substituting the right side of Eqs. (55) and (56) and the left side of Eqs. (55) and (56) to Eq. (60). The parameters μ_k, σ_k, γ_m and κ_2 can be estimated using Matlab software (version 2020), and the best-estimated values were selected according to the minimum value of E. Similar steps were conducted to estimate the parameters for the other two combinations. The estimated values of μ_a, σ_a, μ_k, σ_k, γ_m, κ_2 in the three combinations are shown in Table 7. The estimated values match well with the true ones, which can verify the effectiveness of the estimation method. It should be noted that in the calculation process of left side of Eqs. (55) and (56), 300,000 is assigned to the number of Monte Carlo simulations (N) based on a series of numerical tests.

Furthermore, the size distribution patterns were also verified. μ_k and σ_k were estimated by assuming that the ratio of short-long axis lengths follows the normal distribution, gamma distribution, and uniform distribution, respectively. Taking the trace length on any two sampling windows as an example, $E_1(l^3)/E_2(l^3)$ is a determined value, and $(\rho_1\tau_2)/(\rho_2\tau_1)$ of the ratio of short-long axis lengths in three distribution forms can be obtained (Table 8). According to the results, $g(k)$ can be represented well by the normal distribution, which is consistent with the actual distribution.

When $g(k)$ is determined, $16\tau E(l^3)/(3\pi\rho)$ can be also determined. $E(a^4)/E(a)$ can be estimated by assuming that the length of the long axis follows the negative exponential distribution, gamma distribution, and log-normal distribution, respectively (Table 9). According to the results, $g(a)$ can be represented well by the negative exponential distribution, which is consistent with the actual distribution.

6. Discussion

6.1. Comparison with the existing non-UED and circular disc models

Eqs. (36) and (37) are the universal expression of the mean value and standard deviation of the trace length in the UED model under one sampling window. Both non-UED and circular disc models can be viewed as special forms of the UED model. Hence, the formulae of the mean value and standard deviation of the trace length of the UED model can be simplified as the formulae of the non-UED and circular disc models. The difference between formulae mainly depends on τ, η and $E(k)$.

According to the assumption of the non-UED model (Zhang et al., 2002), the dip direction α, dip angle β, rotation angle γ and ratio of short-long axis lengths k are constant. The angle between the trace line and the long axis (ω) on one sampling window with a dip direction of α_s and a dip angle of β_s is also a constant. Hence, the formulae of the mean value and standard derivation of trace length can be given by

$$\mu_l = \frac{\pi(\mu_a^2+\sigma_a^2)E(k)}{4\sqrt{\frac{\tan^2[\omega(\alpha,\beta,\gamma,\alpha_s,\beta_s)]+k^2}{\tan^2[\omega(\alpha,\beta,\gamma,\alpha_s,\beta_s)]+1}}\mu_a} \tag{67}$$

$$\sigma_l^2 = \frac{2k^2\{\tan^2[\omega(\alpha,\beta,\gamma,\alpha_s,\beta_s)]+1\}E(a^3)}{3\left\{\tan^2[\omega(\alpha,\beta,\gamma,\alpha_s,\beta_s)]+k^2\right\}\mu_a} - \mu_l^2 \tag{68}$$

The expression of ω has not been given in Zhang et al. (2002). The size- and azimuth-related parameter was estimated by trial and error. Zhang et al. (2002) transformed the ratio of long-short axis lengths under different directions of long axis, and then calculate the length of the long axis. When the mean or standard deviation of the length of the long axis in different sampling windows intersected at one point, the corresponding parameters of the point are the desired results. The trial and error method given by Zhang et al. (2002) is complex and time-consuming. Therefore, the derivation of ω in this paper can be used to improve the estimation of the size- and azimuth-related parameters of this non-UED model developed by Zhang et al. (2002) by combing the trace information of any two different sampling windows.

Jin et al. (2014) considered the variance of orientation in Zhang's assumption (Zhang et al., 2002) and concluded that the distribution of trace length is independent of the orientations of the sampling windows and fractures. Based on the derivation of ω in Appendix A, the value of ω varies with the orientations of the sampling windows and fractures. When the orientation of the elliptical disc model is a variable, ω is no longer a constant, and its distribution is also related to the distribution of orientations. Unfortunately, Jin et al. (2014) did not establish the relationship between ω and fracture orientations and considered ω as a constant. Therefore, based on the

Table 8
The ratio of short-long axis lengths in different distributions.

$E_1(l^3)/E_2(l^3)$	$(\rho_1\tau_2)/(\rho_2\tau_1)$		
	Normal distribution	Gamma distribution	Uniform distribution
1.455	1.44	1.49	1.171

Table 9
The length of the long axis in different distributions.

$16\tau E(l^3)/3\pi\rho$	$E(a^4)/E(a)$		
	Negative exponential distribution	Gamma distribution	Log-normal distribution
96	95.2	210.4	187.4

Table 10
The parameters and characteristics in the rectangular disc model.

Rectangular fracture	Distribution	Parameter
Density		$1/m^3$
Location	Poisson distribution	
Long side length (m)	Exponential distribution	Mean value: 2, standard deviation: 2
Ratio of the short to long sides	Normal distribution	Mean value: 0.4, standard deviation: 0.1
Orientation	Fisher distribution	$\kappa_1 = 15$, $\alpha_m = 60^\circ$ and $\beta_m = 150^\circ$
Rotation angle	Von Mises distribution	$\kappa_2 = 10$ and $\beta_m = 30^\circ$

Table 11
The true mean value and standard deviation of trace length in three sampling windows.

Orientation of sampling windows (δ_s (°)/θ_s (°))	True mean value	True standard deviation
30/60	1.528	1.325
15/210	1.746	1.715
60/330	1.622	1.487

Table 12
The estimated parameters of the circular disc, non-UED and UED models.

Model	Distributions and parameter
Circular disc model	Radius (m): Exponential distribution, mean value is 1.04 and standard deviation is 1.04
Non-UED model	Length of the long axis (m): Exponential distribution, mean value is 3.79 and standard deviation is 3.79; Ratio of short-long axis lengths: Constant value of 0.24 Rotation angle: Constant value of 22.3°
UED model	Length of the long axis (m): Exponential distribution, mean value is 2.45 and standard deviation is 2.45; Ratio of short-long axis lengths: Normal distribution, mean value is 0.35 and standard deviation is 0.1; Rotation angle: Von Mises distribution: $\kappa_2 = 9.7$ and $\beta_m = 26.5^\circ$

derivations in this study, the formulae of trace length of the non-UED model considering the variance of fracture orientations in Jin et al. (2014) can be written as

$$\mu_l = \frac{\pi(\mu_a{}^2 + \sigma_a^2)E(k)}{4\tau\mu_a} \tag{69}$$

$$\sigma_l^2 = \frac{2\eta E(a^3)}{3\tau\mu_a} - \mu_l^2 \tag{70}$$

where

$$\tau = \int_0^{2\pi}\int_0^{\pi}\sqrt{\frac{\tan^2[\omega(\alpha,\beta,\gamma,\alpha_s,\beta_s)]+k^2}{\tan^2[\omega(\alpha,\beta,\gamma,\alpha_s,\beta_s)]+1}}f(\alpha,\beta)\mathrm{d}\alpha\mathrm{d}\beta \tag{71}$$

$$\eta = \int_0^{2\pi}\int_0^{\pi}k^2\sqrt{\frac{\tan^2[\omega(\alpha,\beta,\gamma,\alpha_s,\beta_s)]+1}{\tan^2[\omega(\alpha,\beta,\gamma,\alpha_s,\beta_s)]+k^2}}f(\alpha,\beta)\mathrm{d}\alpha\mathrm{d}\beta \tag{72}$$

For the circular disc model, the size- and azimuth-related variables include only diameter and orientation. Since $k = 1$, the values of τ and η are also equal to 1. The formulae of the mean value and standard deviation of the circular disc model can be expressed as

$$\mu_l = \frac{\pi\left(\mu_d^2 + \sigma_d^2\right)}{4\mu_d} \tag{73}$$

$$\sigma_l^2 = \frac{2E\left(d^3\right)}{3\mu_d} - \mu_l^2 \tag{74}$$

where d is the diameter in the circular disc model; and μ_d and σ_d are the mean and standard deviation of the d, respectively. It is consistent with the formulae of the circular disc models developed by Zhang and Einstein (2000).

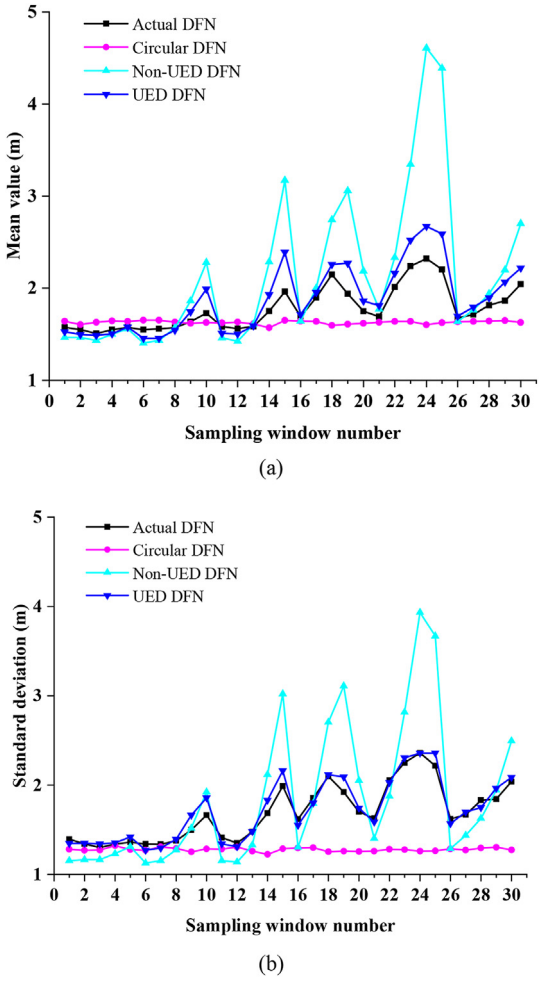

Fig. 7. Mean value and standard deviation of the trace length of 3D DFNs in the four models: (a) Mean value, and (b) Standard deviation.

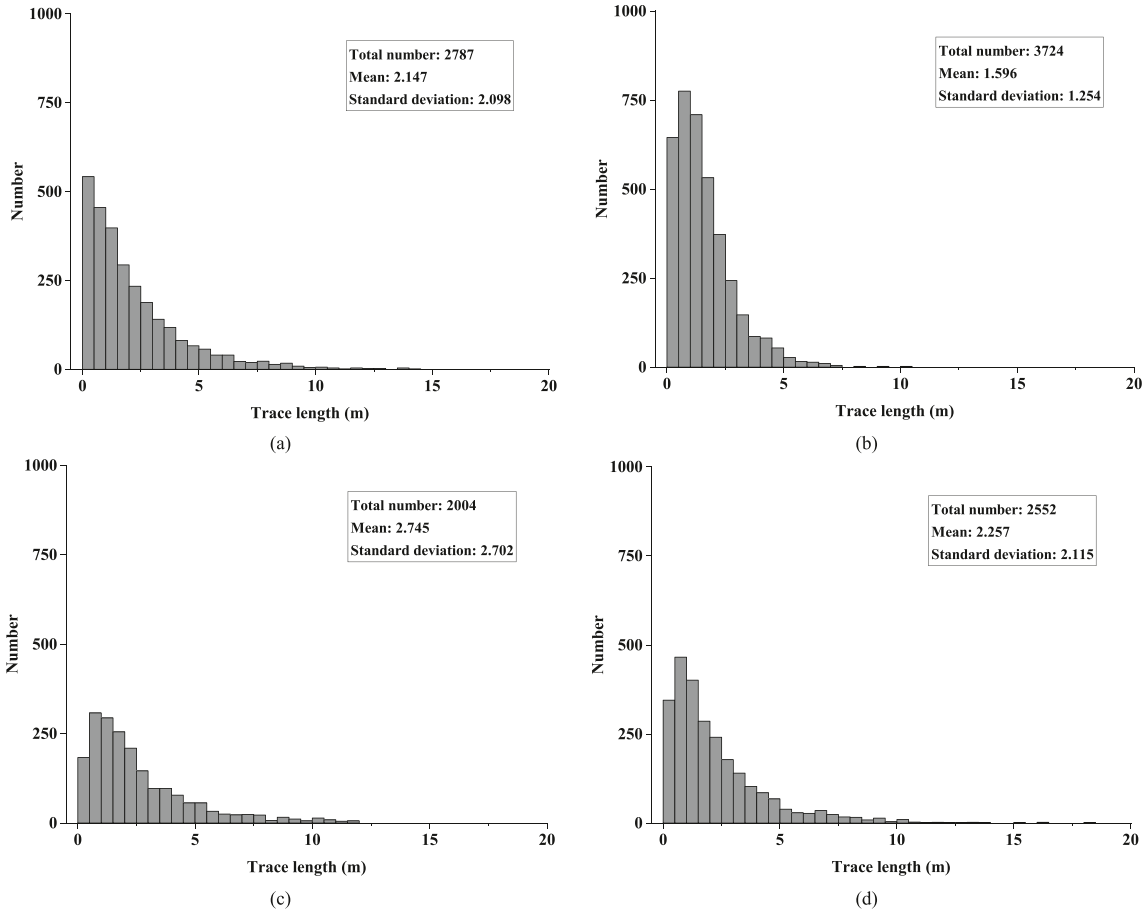

Fig. 8. Histograms of frequency distributions for the trace length of 3D DFNs in the four models: (a) Actual DFN, (b) Circular disc DFN, (c) Non-UED DFN, and (d) UED DFN.

To further compare the circular disc, non-UED and UED models, a hypothetical case study of 3D rectangular DFN was constructed in a block via Monte Carlo simulations, and its geometric characteristics are shown in Table 10. The block size is 50 m × 50 m × 50 m (length × width × height), with 125,000 rectangular fractures. Three infinite sampling windows with different orientations were used to collect the trace length, and the results are given in Table 11.

The hypothetical case study is viewed as the actual DFN, which is represented in the circular disc model, non-UED model and UED model, respectively. It should be noted that when the fracture orientation is constant, the traces are parallel, and it is inconsistent with the actual rock mass. Hence, only the non-UED model with the variance of orientation has been used. According to the trace information shown in Table 11, the parameters of the UED model and non-UED model can be estimated based on the aforementioned optimization method. The diameter of the circular disc model can be computed by Eqs. (73) and (74) based on the average of the mean value and standard deviation of the traces in three sampling windows. The estimated parameters of the three models are shown in Table 12. According to the estimated parameters, the 3D DFNs of the circular disc, non-UED and UED models can be generated.

Thirty infinite sampling windows were used to collect the trace lengths of the actual DFN, circular disc DFN, non-UED DFN, and UED DFN. The orientations of these thirty sampling windows are consistent with those listed in Table 3. The mean value and standard deviation of the trace lengths of DFNs of the four types are shown in Fig. 7. The results in Fig. 7 clearly show that (1) with respect to the circular DFN, the mean value and standard deviation of trace length in different sampling windows are almost the same, indicating that the circular DFN cannot reflect the trend of mean value and standard deviation of trace length in different sampling windows. This is consistent with the results in Eqs. (73) and (74); (2) the non-UED DFN can reflect the trend of the mean value and standard deviation of trace length in different sampling windows; however, the error rates are high, e.g. the maximum error rates of the mean value and standard deviation of trace length for all sampling windows are 99.5% and 66.7%, respectively; (3) the UED model can well reflect the trend of the mean value and standard deviation of trace length in different sampling windows. The maximum error rates of the mean of trace length for all sampling windows are 20.9% and 11.8%, respectively, which are much less than those of the non-UED DFN; and (4) the simulated traces based on the UED model are closest to the actual ones. The frequency distribution histograms of the trace length of DFNs of the four types in the sampling window with a dip direction of 180° and a dip angle of 45° are shown in Fig. 8. It can be seen that the total number, mean, standard deviation and frequency distribution histogram of the trace length in the UED model are closest to those of the actual rock mass. The comparison results clearly illustrate that UED model outperforms the circular disc and non-UED models.

6.2. Future work on the UED model

Compared with the formulae of trace length in elliptical disc models, a significant feature of the circular disc model is that the mean value and standard deviation of trace length are independent of sampling windows, i.e. the mean value and standard deviation of the circular disc model are constant in all sampling windows.

Hence, the trace length in different sampling windows can be used as the criterion for model selection. When there are large differences in trace length in different sampling windows, the fractures must not be equidimensional discs, and the circular disc model is inapplicable.

In Section 3.2, the true values of the mean and standard deviation of trace length obtained from the Monte Carlo simulations are close to the calculated values computed by Eqs. (36) and (37). It should be noted that the true values of trace length are collected from the infinite sampling window; while in an actual rock mass, it was obtained based on a finite sampling window. In a finite sampling window, trace errors may occur due to biases including orientation, size, truncation and censoring (Kulatilake and Wu, 1984; Zhang and Einstein, 2000). How to obtain the mean value and standard deviation of the trace length for the UED model based on a finite sampling window is worth studying in the future.

In Section 3, it can be concluded that the distribution of trace length depends on the distributions of the orientation, rotation angle, length of the long axis, and the ratio of short-long axis lengths of the UED model. The relationship between the trace length and the size and azimuth distributions has not been investigated thoroughly. In the future, based on the combination of the common distributions of size and azimuth, we will study the distribution of trace length under different sampling windows. Even if it is impossible to directly estimate the size and orientation distributions from the trace distribution, it may help eliminate unrealistic size and azimuth distributions.

It should be noted that the proposed method of parameter estimation of the UED model requires three sampling windows. This method is mainly applied to complicated underground engineering where three sampling windows can be provided, such as underground power plants or underground coal mines. For a general tunnel or a slope, three sampling windows are usually uneasy to obtain; hence, the proposed method is not applicable. In the future, the parameter estimation of the UED model will be improved by combining the data of sampling windows and boreholes to improve its adaptability.

7. Conclusions

The stereological relationship between the distributions of trace length, size (length of the long axis and ratio of short-long axis lengths) and azimuth (orientation and rotation angle) of the UED model has been established, and the formulae of mean value and standard deviation of the trace length of Eqs. (36) and (37) on one sampling window were proposed. The validation of Eqs. (36) and (37) was performed, and the results (Fig. 5) show that the calculated values are in good agreement with the true ones, and the *ER*s of the mean value and standard deviation of trace length are less than 5%. Hence, the proposed formulae are valid. Concerning parameter estimations, the distributions of the geometric characteristics were first assumed. The method of Monte Carlo simulation was applied to solving the complex integral, and the optimization algorithm can be used to estimate the parameters based on the trace length from multiple sampling windows. With respect to the suitability of the assumed size distribution forms, the third moment of the trace length distribution was proposed with the azimuth distribution fixed. The procedures of estimating the size- and azimuth-related parameters of the UED model were summarized in Fig. 6.

In order to validate and apply the size- and azimuth-related parameter estimation, the trace lengths from three different combinations of sampling windows were used. The results (Table 7) showed that the estimated values were close to the true values, and the mean error rate is less than 9.2%, and hence the proposed method of parameters estimation is valid. Furthermore, the distribution forms of the size-related parameters were also checked based on the third moment of the trace length, and the results (Tables 8 and 9) showed that the best distribution forms are consistent with the actual distribution forms of the size-related parameters.

Compared with the existing non-UED and circular disc models, the formulae of the trace length of the UED model were discussed. The formulae of the UED model can be reduced to the non-UED and circular disc models, which can further validate the proposed equations of the UED model. A hypothetical 3D rectangular fracture network was constructed using the circular disc, non-UED and UED models. The trace information of the three models was compared with the actual rock mass (Figs. 7 and 8), and the results clearly illustrate the superiority of the UED model over the circular disc and non-UED models.

Declaration of competing interest

The authors declare that they have no known competing financial interests or personal relationships that could have appeared to influence the work reported in this paper.

Acknowledgments

This study was funded by National Natural Science Foundation of China (Grant No. 41972264), Zhejiang Provincial Natural Science Foundation of China (Grant No. LR22E080002), and the Observation and Research Station of Geohazards in Zhejiang, Ministry of Natural Resources, China (Grant No. ZJDZGCZ-2021).

Appendix A. Supplementary data

Supplementary data to this article can be found online at https://doi.org/10.1016/j.jrmge.2022.07.018.

References

Ajayi, K.M., Schatzel, S.J., 2020. Transport model for shale gas well leakage through the surrounding fractured zones of a longwall mine. Int. J. Min. Sci. Technol. 30 (5), 635–641.
Baecher, G.B., Lanney, N.A., Einstein, H.H., 1977. Statistical description of rock properties and sampling. In: Proceedings of the 18th U.S. Symposium on Rock Mechanics. ARMA-77-0400.
Baghbanan, A., Jing, L., 2007. Hydraulic properties of fractured rock masses with correlated fracture length and aperture. Int. J. Rock Mech. Min. Sci. 44, 704–719.
Barton, C.M., 1978. Analysis of joint traces. In: Proceedings of the 19th U.S. Symposium on Rock Mechanics, p. 3841.
Bingham, C., 1974. An antipodally symmetric distribution on the sphere. Ann. Stat. 2, 1201–1225.
Cacas, M.C., Ledoux, E., Demarsily, G., et al., 1990. Modeling fracture flow with a stochastic discrete fracture network: calibration and validation: 1. The flow model. Water Resour. Res. 26 (3), 479–489.
Chen, D., Chen, H., Zhang, W., Lou, J., Shan, B., 2021. An analytical solution of equivalent elastic modulus considering confining stress and its variables sensitivity analysis for fractured rock masses. J. Rock Mech. Geotech. Eng. https://doi.org/10.1016/j.jrmge.2021.08.007.
Chilès, J.P., 1988. Fractal and geostatistical methods for modeling of a fracture network. Math. Geol. 20 (6), 631–654.
Dershowitz, W.S., Einstein, H.H., 1988. Characterizing rock joint geometry with joint system models. Rock Mech. Rock Eng. 21, 21–51.
Evans, M., Swartz, T., 2000. Approximating Integrals via Monte Carlo and Deterministic Methods. Oxford University Press, New York, USA, p. 1287.
Fan, X., Yang, Z., Li, K., 2021. Effects of the lining structure on mechanical and fracturing behaviors of four-arc shaped tunnels in a jointed rock mass under uniaxial compression. Theor. Appl. Fract. Mech. 112, 102887.
Fisher, N.I., Lewis, T., Embleton, B.J.J., 1987. Statistical Analysis of Spherical Data. Cambridge University Press, Cambridge, UK.
Gao, M., Jin, W., Zhang, R., Xie, J., Yu, B., Duan, H., 2016. Fracture size estimation using data from multiple boreholes. Int. J. Rock Mech. Min. Sci. 86, 29–41.
Guo, J., Zheng, J., Lü, Q., Cui, Y., Deng, J., 2020. A procedure to estimate the accuracy of circular and elliptical discs for representing the natural discontinuity facet in the discrete fracture network models. Comput. Geotech. 121, 103483.

Guo, J., Zheng, J., Lü, Q., Sun, H., 2021. Empirical methods to quickly select an appropriate discrete fracture network (DFN) model representing the natural fracture facets. Bull. Eng. Geol. Environ. 80, 5797–5811.
ISRM, 1978. International society for rock mechanics commission on standardization of laboratory and field tests: suggested methods for the quantitative description of discontinuities in rock masses. Int. J. Rock Mech. Min. Sci. Geomech. Abstr. 15, 319–368.
Ivanova, V., 1998. Geologic and Stochastic Modeling of Fracture Systems in Rocks. Massachusetts Institute of Technology, Cambridge, MA, USA.
Jin, W., Gao, M., Zhang, R., Zhang, G., 2014. Analytical expressions for the size distribution function of elliptical joints. Int. J. Rock Mech. Min. Sci. 70, 201–211.
Kemeny, J., Post, R., 2003. Estimating three-dimensional rock discontinuity orientation from digital images of fracture traces. Comput. Geosci. 29, 65–77.
Kulatilake, P.H.S.W., Wu, T.H., 1984. Estimation of mean trace length of discontinuities. Rock Mech. Rock Eng. 17 (4), 215–232.
Kulatilake, P.H.S.W., 1986. Bivariate normal distribution fitting on discontinuity orientation clusters. Math. Geol. 18, 181–195.
Kulatilake, P.H.S.W., Wu, T.H., Wathugala, D.N., 1990. Probabilistic modelling of joint orientation. Int. J. Numer. Anal. Model. 14, 325–350.
Kulatilake, P.H.S.W., Wathugala, D.N., Stephansson, O., 1993. Joint network modeling with a validation exercise in Stripa mine, Sweden. Int. J. Rock Mech. Min. Sci. Geomech. Abstr. 30 (5), 503–526.
Kulatilake, P.H.S.W., He, W., Um, J., Wang, H., 1997. A physical model study of jointed rock mass strength under uniaxial compressive loading. Int. J. Rock Mech. Min. Sci. 34, 165 e1–165.e15.
Li, Z., Lu, B., Zou, J., Xu, B., Zhang, Z., 2016. Design and operation problems related to water curtain system for underground water-sealed oil storage caverns. J. Rock Mech. Geotech. Eng. 8 (5), 689–696.
Ma, K., Liu, G., 2022. Three-dimensional discontinuous deformation analysis of failure mechanisms and movement characteristics of slope rockfalls. Rock Mech. Rock Eng. 55, 275–296.
Pan, P., Wu, Z., Feng, X., Yan, F., 2016. Geomechanical modeling of CO_2 geological storage: a review. J. Rock Mech. Geotech. Eng. 8, 936–947.
Petit, J.-P., Massonnat, G., Pueo, F., Rawnsley, K., 1994. Rapport de forme des fractures de mode 1 dans les roches stratifiees: une etude de cas dans le Bassin Permian de Lodeve (France). Bull. Cent. Rech. Elf Explor. Prod. 18, 211–229 (In French).
Priest, S.D., 1993. Discontinuity Analysis for Rock Engineering. Chapman & Hall, London, UK.
Priest, S.D., 2004. Determination of discontinuity size distributions from scanline data. Rock Mech. Rock Eng. 37 (5), 347–368.
Song, J.J., 2006. Estimation of a joint diameter distribution by an implicit scheme and interpolation technique. Int. J. Rock Mech. Min. Sci. 43, 512–519.
Shaunik, D., Singh, M., 2020. Bearing capacity of foundations on rock slopes intersected by non-persistent discontinuity. Int. J. Min. Sci. Technol. 30 (5), 69–674.
Villaescusa, E., Brown, E.T., 1992. Maximum likelihood estimation of joint size from trace length measurements. Rock Mech. Rock Eng. 25 (2), 67–87.
Warburton, P.M., 1980a. A stereological interpretation of joint trace data. Int. J. Rock Mech. Min. Sci. Geomech. Abstr. 17 (4), 181–190.
Warburton, P.M., 1980b. Stereological interpretation of joint trace data: influence of joint shape and implications for geological surveys. Int. J. Rock Mech. Min. Sci. Geomech. Abstr. 17 (6), 305–316.
Wu, Q., Kulatilake, P.H.S.W., Tang, H., 2011. Comparison of rock discontinuity mean trace length and density estimation methods using discontinuity data from an outcrop in wenchuan area, China. Comput. Geotech. 38 (2), 258–268.
Zhang, L., Einstein, H.H., 2000. Estimating the intensity of rock discontinuities. Int. J. Rock Mech. Min. Sci. 37 (5), 819–837.
Zhang, L., Einstein, H.H., Evans, W.S., 2002. Stereological relationship between trace length and size distribution of elliptical discontinuities. Geotechnique 52 (6), 419–433.
Zhang, L., Einstein, H.H., 2010. The planar shape of rock joints. Rock Mech. Rock Eng. 43 (1), 55–68.
Zhang, W., Fu, R., Tan, C., et al., 2020. Two-dimensional Discrepancies in fracture geometric factors and connectivity between field-collected and stochastically modeled DFNs: a case study of sluice foundation rock mass in Datengxia, China. Rock Mech. Rock Eng. 53, 2399–2417.
Zhang, B., Mu, J., Zheng, J., Lü, Q., Deng, J., 2021. A new estimation method and an anisotropy index for the deformation modulus of jointed rock masses. J. Rock Mech. Geotech. Eng. 14 (1), 153–158.
Zheng, J., Kulatilake, P.H.S.W., Shu, B., Sherizadeh, T., Deng, J., 2014a. Probabilistic block theory analysis for a rock slope at an open-pit mine in USA. Comput. Geotech. 61, 254–265.
Zheng, J., Deng, J., Yang, X., Wei, J., Zheng, H., Cui, Y., 2014b. An improved Monte Carlo simulation method for discontinuity orientations based on Fisher distribution and its program implementation. Comput. Geotech. 61 (3), 266–276.
Zheng, J., Zhao, Y., Lü, Q., Deng, J., Chen, R., 2017. Estimation of the three-dimensional density of discontinuity systems based on one-dimensional measurements. Int. J. Rock Mech. Min. Sci. 94, 1–9.
Zheng, J., Wang, X., Lü, Q., Sun, H., Guo, J., 2020. A new determination method for the permeability tensor of fractured rock masses. J. Hydrol. 585, 124811.
Zheng, J., Guo, J., Wang, J., Sun, H., Deng, J., Lü, Q., 2022. A universal elliptical disc (UED) model to represent natural rock fractures. Int. J. Min. Sci. Technol. 32 (2), 261–270.

Jun Zheng is an Associate Professor and a doctoral supervisor in College of Civil Engineering and Architecture at Zhejiang University. He obtained his Joint PhD in geotechnical engineering from Sichuan University (China) and the University of Arizona (USA) in 2014. He was a Visiting Scholar at Delft University of Technology in 2016. His research interests are in rock mechanics and geohazard prevention and mitigation, particularly including (1) geometric model and computer simulation of rock mass structures, (2) relationship between geometric model and mechanical behaviors of rock masses, (3) application of artificial intelligence in rapid acquisition of geometric parameters of rock discontinuities, and (4) probabilistic stability analysis of rock masses. He is responsible for two projects sponsored by the National Natural Science Foundation of China, and has published over 70 scientific papers. Dr. Zheng has won several awards including Excellent Doctoral Dissertation Award of Chinese Society for Rock Mechanics and Engineering (CSRME) in 2016 and Natural Science Award of CSRME in 2018. He was selected in the Young Elite Scientists Sponsorship Program by China Association for Science and Technology (CAST) in 2018. He is serving as a young editorial board member of an international journal and two domestic journals, and has served as a reviewer for about 30 rock mechanics/geotechnical/engineering geology journals.